# Cylindrical Surface Reconstruction by Fitting Paths on Shape Space

Chafik Samir
chafik.samir@udamail.fr
ISIT CNRS UMR 6482, University of Clermont, France.
Pierre-Yves Gousenbourger
pierre-yves.gousenbourger@uclouvain.be
ICTEAM, Université catholique de Louvain, 1348 Louvain-la-Neuve, Belgium.
Shantanu H. Joshi
s.joshi@g.ucla.edu
UCLA Brain Mapping Center, Department of Neurology, University of California Los Angeles, CA 90095.

**Abstract**

We present a differential geometric approach for cylindrical anatomical surface reconstruction from 3D volumetric data that may have missing slices or discontinuities. We extract planar boundaries from the 2D image slices, and parameterize them by an indexed set of curves. Under the SRVF framework, the curves are represented as invariant elements of a nonlinear shape space. Differently from standard approaches, we use tools such as exponential maps and geodesics from Riemannian geometry and solve the problem of surface reconstruction by fitting paths through the given curves. Experimental results show the surface reconstruction of smooth endometrial tissue shapes generated from MRI slices.

## 1 Introduction

The problem of surface reconstruction from 3D images has been widely studied because of its importance in different applications such as medical imaging, computer graphics, mechanical simulations, virtual reality, etc. Particularly, the reconstruction of surfaces from a set of $3D$ point clouds is important since they are frequently used in medical imaging and computer graphics [3]. For example, one can use a variational formulation using PDEs and compute the solution as an implicit surface, which is usually the zero level set of a sufficiently smooth function [16]. Here, the resulting surface construction is controlled by adding physics-inspired constraints depending on geometry or external forces [16]. However, when the observed data is acquired as 2D image slices, one can often find convenient planar boundary representations of objects of interest. Then one needs to perform surface reconstruction by computing an optimal fitting between the boundaries and taking into account their parametrization and the non-linearity of their spatial evolution [6].

In several medical applications, real data can be partially extracted by an expert (manually), and then used to validate medical image processing algorithms. While modern MR reconstruction algorithms allow the acquisition of full 3D anatomies, often times due the resolution of the imaging device, or position of the anatomical object in the scanner the 3D surface reconstruction during the post-processing phase may be difficult. In such cases the


Pages 11.1-11.10
https://dx.doi.org/10.5244/C.29.DIFFCV.11

physician expert usually traces boundaries on a subset of 2D image slices. The difficulty then lies in generating a surface reconstruction out of the sequence of image slices.

To overcome this issue, we formulate the problem of reconstructing a surface from an acquired set of indexed curves as a smooth path fitting scheme on the shape space. Path fitting on manifolds has been previously addressed in the literature with different approaches and for various purposes. Generic path fitting methods on manifolds include splines on manifolds [10], rolling procedures [7], subdivision schemes [4], gradient descent [13], and geodesic finite elements [14]. Interpolation of rotations (where the manifold $\mathcal{M}$ is the special orthogonal group $SO(3)$) is useful in robotics for motion planning of rigid bodies and in computer graphics for the animation of 3D objects [11]. Although the standard reconstruction approaches produce valid correspondences between given data, there is still a lack for smoothness, which requires arbitrary smoothing schemes.

The main advantages of our proposed path fitting methods are: i) the fitting formulation takes into account the fact that the given data is available as a set of indexed spatial level-set curves and finds the intermediate missing curves under a smoothing constraint, ii) the resulting cylindrical surfaces have a natural parametrization as a path on curves space, and iii) they benefit of an attractive elastic metric to compute the evolution and the deformation along the given level-set curves and between them.

## 2 The Path Fitting Problem on the Euclidean Space

Since the acquired set of 2D curves is an ordered sequence, the main idea here is to connect them as a smooth path of curves to form a continuous surface. Let $p_0, p_1, p_2, \ldots, p_n$ be an indexed set of curves. Our goal is to construct a smooth piecewise-Bézier path $\eta : [0, t_n] \to \mathcal{M}$ interpolating the $n+1$ data points $p_i = \eta(t_i) \in \mathcal{M}$ at time instants $t_i$ for $i = 0, \ldots, n$. In [2, 6], methods to do so were proposed for a general Riemannian manifold $\mathcal{M}$. In both works, the strategy was to formulate a $C^1$ piecewise-Bézier interpolation problem for the case where $\mathcal{M}$ reduces to a Euclidean space, then obtain equations that govern the control points of the sought Bézier curves, and finally generalize those equations to Riemannian manifolds. In this section, we briefly summarize the Euclidean foundations of two of these methods, referring the reader to [6] and [2] for details. Then, in the next section, we work out concretely the extension of the two methods to the specific case where the manifold $\mathcal{M}$ is the shape space of curves.

In the Euclidean case we consider $n+1$ data points $(p_0, \ldots, p_n)$ in $\mathbb{R}^m$ and assume that $n \geq 3$ for non trivial cases. The $C^1$ piecewise-Bézier path $\eta$ is defined as:

$$\eta(t) = \begin{cases} \beta_2(t; p_0, b_1^-, p_1) & t \in [0,1] \\ \beta_3(t-(i-1); p_{i-1}, b_{i-1}^+, b_i^-, p_i) & t \in [i-1, i],\ i = 2, \ldots, n-1 \\ \beta_2(t-(n-1); p_{n-1}, b_{n-1}^+, p_n) & t \in [n-1, n], \end{cases} \tag{1}$$

where $\beta_k$ denotes a Bézier curve of degree $k$ [5] and $(b_i^-, b_i^+)$ are control points on the left and on the right of the data point $p_i$, $i = 1, \ldots, n-1$. The control points are chosen such that the mean square acceleration

$$\int_0^1 (\|\ddot{\beta}_2(t; p_0, b_1^-, p_1)\|^2 + \sum_{i=1}^{n-2} \|\ddot{\beta}_3(t; p_{i-1}, b_{i-1}^+, b_i^-, p_i)\|^2 + \|\ddot{\beta}_2(t; p_{n-1}, b_{n-1}^+, p_n)\|^2) \mathrm{d}t \tag{2}$$

is minimized in $\mathbb{R}^m$.

**Solution 1.** In this method, we assume that the control points $(b_i^-, b_i^+)$ depend on their closest interpolation point $p_i$. We fix the velocity directions $v_i$ at $p_i$ and optimize their magnitude $\alpha_i$, so the control points now read:

$$b_i^+ = p_i + \xi \alpha_i v_i \qquad i = 1, \ldots, n-1 \tag{3}$$

$$b_i^- = p_i - \xi \alpha_i v_i \qquad i = 1, \ldots, n-1 \tag{4}$$

where $\xi = 3/2$ for $b_1^-$ and $b_{n-1}^+$ and 1 otherwise. Minimizing Eqn. 2 turns then into solving a tridiagonal linear system of the form $M\alpha = z$. Control points are then recovered following Eqn. 3 and Eqn. 4 (see [6] for more details).

**Solution 2.** Here, we assume that the control points $b_i^+$ (on the right of $p_i$) depend on the control points on the left $b_i^-$. The minimizer of Eqn. 2 is given as the critical point of its gradient, which leads to a linear system of the form $AX = CP$ including $b_i^-$ only as $X = [b_1^-, \ldots, b_{n-1}^-]^T \in \mathbb{R}^{n-1 \times m}$ and $P = [p_0, \ldots, p_n]^T \in \mathbb{R}^{n+1,m}$. $A$ and $C$ are tridiagonal matrices of coefficients (see [2] for details) with $A$ invertible which makes the solution unique:

$$X = A^{-1}CP. \tag{5}$$

# 3 The Path Fitting Problem on the Shape Space

We now generalize the path fitting problem of section 2 to the shape space. It is worth noting that the solutions presented above can be expressed on some general Riemannian manifolds embedded in a Euclidean space $\mathcal{E}$ [2, 6]. For such a generalization, one needs to define and compute the exponential map, the logarithmic map and an appropriate metric [1, 12].

## 3.1 Shape Analysis of Closed Planar Curves

This section summarizes the Riemannian framework for elastic shape analysis of closed planar curves. This general framework results in metrics and models that are invariant to arbitrary rotation, scaling, translation, and re-parameterization of individual curves. For more detailed information, we refer the reader to [8]. In this work, rotation, translation, and scaling are not considered as nuisance variables because they are derived from real data. We will assume that an arbitrary level-set curve is represented by its parameterization $\beta_i$, its length $l_i$, and its starting point $\beta(0)$. As $l_i$ and $\beta(0)$ belong to Euclidean spaces, their interpolation is quite straightforward. In the following section, we will focus on the interpolation between $\beta_i$s.

### 3.1.1 Representation of Curves

We represent the shape of a two-dimensional parameterized curve $\beta$, $\beta : [0,1] \to \mathbb{R}^n$ by a function [8, 15] $q : [0,1] \to \mathbb{R}^n$ as

$$q(s) = \frac{\dot{\beta}(s)}{\sqrt{||\dot{\beta}(s)||_{\mathbb{R}^n}}} \in \mathbb{R}^n. \tag{6}$$

This vector valued function $q$ is the tangent vector normalized by the square-root of the instantaneous speed along the curve and is a local descriptor of the geometry of the curve. The

original curve $\beta$ can be reconstructed using $\beta(s) = \beta(0) + \int_0^s ||q(t)||\, q(t)\, dt$. Since this operation maps the shape space representation of a curve to its representation in a system with coordinates, we denote it as $\mathbf{coord}(q)$, *i.e.* $\beta = \mathbf{coord}(q)$, given $\beta(0)$. The scale invariant shape representation is given by normalizing the function $q$ by its magnitude as $\frac{q}{\sqrt{\int_0^1 (q(s),q(s))_{\mathbb{R}^2} ds}}$. The norm in the denominator is a Euclidean norm, and $(\cdot,\cdot)_{\mathbb{R}^2}$ is the standard Euclidean inner-product in $\mathbb{R}^2$. Throughout this section, the function $q$ refers to this scale-invariant form unless indicated otherwise. Due to this unit-scaling constraint, the space of all translation and scale-invariant shapes becomes a Hilbert sphere denoted by $\mathcal{Q}$. Formally, the space $\mathcal{Q}$ is defined as

$$\mathcal{Q} \equiv \left\{ q \in \mathbb{L}^2 | \int_0^1 (q(s),q(s))_{\mathbb{R}^2} ds = 1, q(s) : [0,1] \to \mathbb{R}^2 \right\}. \tag{7}$$

Ultimately, we are interested in analyzing curves in a fully invariant manner, *i.e.* we would like to consider an invariant space of shapes given by the quotient space modulo *shape-preserving* transformations including reparameterizations. This invariance to reparameterization is the most interesting shape-preserving transformation and facilitates elastic shape analysis of curves. Reparameterization gives rise to a change in speed of the curve without changing its shape. It is represented by a non-linear differentiable map (with a differentiable inverse) also referred to as a diffeomorphism, which is defined as $\gamma \in \Gamma$, where $\Gamma = \{\gamma : [0,1] \to [0,1], \gamma(0) = 0, \gamma(1) = 1, \gamma \text{ is a diffeomorphism}\}$. One can specify the action of reparameterization of a shape $q$ by $\gamma$ denoted by

$$q \cdot \gamma = (\, q \circ \gamma) \sqrt{\dot{\gamma}}. \tag{8}$$

### 3.1.2 Shape Space of Curves

The elastic shape space of open curves is defined as the quotient space,

$$\mathcal{S}_o = \mathcal{Q}/(\Gamma). \tag{9}$$

This framework also allows us to represent closed boundaries ($\beta : [0,1] \to \mathbb{R}^2$) of objects by imposing an additional closure constraint on the curves. This closure constraint is written as $\int_0^1 \dot{\beta}(s) ds = 0$ and is specified as $\int_0^1 q(s)||q(s)||ds = 0$ in terms of the shape function. One can then define the set of closed representations as the pre-shape space of the curve shapes and denote it by $\mathcal{C} \equiv \{q | q \in \mathcal{Q}, \int q(s)||q(s)||ds = 0\}$. This pre-shape space $\mathcal{C}$ is a subset of an infinite-dimensional unit-sphere as a result of the scale-invariant constraint and represents all closed elastic curves. The elastic shape space for closed curves is then given by the quotient space $\mathcal{S}_c = \mathcal{C}/(\Gamma)$. Next, we present geometric properties on Q and we refer to [15] for equivalent tools on $\mathcal{S}_c$. An important geometrical construct for the statistical analysis of the shapes is the definition of a tangent space. The tangent space of $\mathcal{Q}$ is given by

$$T_q(\mathcal{Q}) \equiv \left\{ f \in \mathbb{L}^2 | f \perp \mathcal{Q} \right\}. \tag{10}$$

We equip the tangent spaces of $\mathcal{Q}$ with a smoothly varying Riemannian metric that measures infinitesimal lengths on the pre-shape space. This inner product is first defined generally on $\mathbb{L}^2$ and then induced on the tangent space of $\mathcal{Q}$. Given a pair of tangent vectors $f, g \in T_q(\mathcal{Q})$ the metric is defined as,

$$\langle f, g \rangle = \int_0^1 (f(s), g(s))_{\mathbb{R}^2} ds. \tag{11}$$

Since this metric is fully invariant to reparameterizations, it is an elastic metric on the shape space of curves.

### 3.1.3 Exponential Map and Inverse Exponential Map on the Shape Space

To enable interpolations between two curves, we use geodesics or shortest paths between them on the shape space. A fundamental ingredient for computing geodesics is the formulation of the exponential map which traces the path of a tangent vector at a given point. Thus given a shape $q_1$ and a tangent vector $f \in T_q(\mathcal{Q})$, the exponential map of $f$ yields a new shape $q_2$ and is defined as

$$\exp_{q_1}(f) = q_2 = \cos(\|f\|)q_1 + \sin(\|f\|)\frac{f}{\|f\|}, \tag{12}$$

where $\|f\| = \langle f, f\rangle$. The shortest path following this tangent vector $f$ and connecting the shapes $q_1$ and $q_2$ is also known as the geodesic. The length of the geodesic determines an elastic quantitative distance between two shapes, whereas the full geodesic path achieves a continuous elastic deformation between them. The geodesic is computed under the Riemannian metric defined in Eqn. 11. Since the space $\mathcal{Q}$ is a Hilbert sphere, the geodesic between two points (shapes) $q_1$ and $q_2$ can be expressed analytically as,

$$\chi_t(q_1; f) = \cos\left(t\cos^{-1}\langle q_1, q_2\rangle\right) q_1 + \sin\left(t\cos^{-1}\langle q_1, q_2\rangle\right) f, \tag{13}$$

where $t \in [0,1]$ and the initial tangent vector $f \in T_{q_1}(\mathcal{Q})$. Conversely, given two shapes $q_1$ and $q_2$, the inverse exponential map (also known as the logarithmic map) allows the recovery of the tangent vector $f$ between them, and is given by

$$\exp_{q_1}^{-1}(q_2) = f = \frac{\cos^{-1}\langle q_1, q_2\rangle}{\sin(\cos^{-1}\langle q_1, q_2\rangle)}\left(q_2 - \langle q_1, q_2\rangle q_1\right). \tag{14}$$

From Eqn. 13, the velocity vector along the geodesic path $\chi_t$ is obtained as $\dot{\chi}_t$. It is also noted that $\chi_0(q_1) = q_1$, and $\chi_1(q_1) = \exp_{q_1}(f) = q_2$. The geodesic is computed using a path-straightening method [8, 15] that initially connects the two points $q_1$ and $q_2$ using an arbitrary path in $\mathcal{Q}$ and then iteratively straightens it to form the shortest path.

The optimal reparameterization $\gamma^*$ at each step can be efficiently found as the minimizer

$$\gamma^* = \underset{\gamma}{\operatorname{argmin}}\left(\int_0^1 \left[||q_1 - \gamma\cdot q_2||^2\right] ds\right), \tag{15}$$

and is numerically solved using dynamic programming. The geodesic path is then given by substituting $q_2$ by $q_2\cdot\gamma^*$ in Eqn. 13, and the tangent vector is given by $\dot{\chi}_0$.

Given the above tools for constructing geodesics and inverse exponential maps on the shape space, we outline their usage in reconstructing cylindrical surfaces from curve shapes next.

## 3.2 Cylindrical Surfaces as Smooth Paths on the Shape Space

Again, given an indexed set of curves $(p_0, p_1, p_2, \ldots, p_n)$ in $\mathbb{R}^2$, we represent their shapes as a set of indexed shape functions $(q_0, q_1, q_2, \ldots, q_n)$ in the shape space $\mathcal{Q}$. The manifold equivalent form of $b_i^+ = p_i + \alpha_i(b_i^- - p_i)$ is then given by the geodesic Eqn. 13 $b_i^+ = \chi_t(q_i; \alpha_i f_i)$, where $q_i$ is a shape and $f_i = \exp_{q_1}^{-1}(b_i^-) \in T_{q_i}(\mathcal{Q})$ is the initial velocity of its geodesic satisfying $\chi_1(q_i; f_i) = b_i^-$.

**Solution 1.** In the first method, given the velocity directions by the tangent vectors $v_i \in T_{q_i}(\mathcal{Q})$, the entries of the matrix $M$ and the vector $z$ are generated as follows:

$$\begin{aligned} M_{(1,1:2)} &= \begin{bmatrix} 12\langle v_1, v_1\rangle & 3\langle v_2, v_1\rangle \end{bmatrix} \\ M_{(i,i-1:i+1)} &= \begin{bmatrix} \langle v_{i-1}, v_i\rangle & 4\langle v_i, v_i\rangle & \langle v_{i+1}, v_i\rangle \end{bmatrix} \\ M_{(n-1,n-2:n-1)} &= \begin{bmatrix} 3\langle v_{n-2}, v_{n-1}\rangle & 12\langle v_{n-1}, v_{n-1}\rangle \end{bmatrix} \end{aligned} \tag{16}$$

and

$$\begin{aligned} z_{(1)} &= 3\langle \exp_{q_1}^{-1}(q_2), v_1\rangle - 2\langle \exp_{q_1}^{-1}(q_0), v_1\rangle \\ z_{(i)} &= \langle \exp_{q_i}^{-1}(q_{i+1}) - \exp_{q_i}^{-1}(q_{i-1}), v_i\rangle \\ z_{(n-1)} &= 3\langle \exp_{q_{n-1}}^{-1}(q_{n-2}), v_{n-1}\rangle - 2\langle \exp_{q_{n-1}}^{-1}(q_n), v_{n-1}\rangle \end{aligned} \tag{17}$$

As each entry is scalar, the magnitudes $\alpha_i$ will remain a vector of scalars and the control points are recovered using $\chi_t(q_i; \pm\alpha_i v_i) = b_i^{\pm}$.

**Solution 2.** The second method is generalized as follow: for each row $i$ of (5), the rest of the data points are mapped to the tangent space $T_{q_i}(\mathcal{Q})$ at $q_i$, *i.e.* $\tilde{P} = [f_1^i, \ldots, f_n^i] \in T_{q_i}(\mathcal{Q})^n$ with $f_k^i = \exp_{q_i}^{-1}(q_k)$. We denote $\tilde{x}_i \in T_{q_i}(\mathcal{Q})$ the solution on the tangent space and $b_i^- = \chi_1(q_i; \tilde{x}_i) \in \mathcal{Q}$ its transported image by the exponential map on $\mathcal{Q}$.

For both solutions, the piecewise-Bézier path is reconstructed on the shape space $\mathcal{Q}$ with the De Casteljau algorithm generalized to manifolds [9] for a certain discretization rate. Since each point of this discrete path belongs to $\mathcal{Q}$, its coordinate representation is obtained as $\mathbf{coord}(\eta(t)),\ \forall t$.

# 4 Experimental Results

In this section, we apply the above methods to reconstruct endometrial tissue surfaces from MRI Slices. Axial T2 MR slices with thickness of 5 mm, repetition time of $44083 - 49397$ ms were acquired with a 1.5 Tesla GE Optima GEM Suite. MR imaging was performed in order to provide superior anatomical details. In our experiments, the MR images had an average size of $400 \times 400 \times 5$ with a voxel resolution of $0.5 \times 0.5 \times 5$ mm$^3$. An expert identified and selected MR slices and then extracted level-set curves. The segmentation was performed by a pelvic radiologist and then confirmed with a gynaecologist.

We present two examples of cylindrical surface reconstruction and compare the fitting paths on shape space obtained with (i) the solution from [2], (ii) the solution from [6] and (iii) a piecewise-geodesics method. The level-set curves were segmented manually by an expert from MRI slices. The selected zones of interest are planar closed curves with constant $z$-value at each level. Examples of extracted level-sets are shown in figures (1 and 2)(a).

To summarize, we reconstruced the smooth endometrial surface $S_{MRI}$ in three steps. First, a radiologist was asked to select different slices (from 4 to 7) and segment curves as boundaries of an interest zone on each slice. Second, we represented each curve as a point on the shape manifold. Note that we aligned and fixed the starting point of each curve and computed its length. The given time indexes, that have spatial meaning in this case, correspond to the $z$-values for each curve from its corresponding slice. Third, thanks to a modified version of [15] to compute a geodesic path between any two points on shape space, we applied the three

methods to construct $S_{MRI}$, for each example. The solution from [2] corresponds to the first two rows, [4] to the rows 3 and 4 and piecewise-geodesics to rows 5 and 6. To give an idea about the quality of the reconstructed surface, we show an example of $S_{MRI}$ (b) reconstructed from a set of curves (a), the norm of the fitting path's velocity $\|\dot{\eta}(t)\|$ (c), the norm of its acceleration $\|\ddot{\eta}(t)\|$ (d) , the Laplacian map $\|\Delta S_{MRI}\|$ (e), the norm of the gradient along the radial curves $\|\nabla_r S_{MRI}\|$ (f), the norm of the gradient along the circular curves $\|\nabla_\theta S_{MRI}\|$ (g), and $\|\nabla_{r,\theta} S_{MRI}\|$ as a function (2D map) of $(r,\theta)$ (h).

One can observe that the three methods are interpolating the given level-set curves as key points on shape space (see figures 1 and 2, left column). Note that the piecewise-geodesic method is continuous but not differentiable at the key points. Moreover, its resulting path has a low velocity cost between any two original curves which is due to the geodesic connecting them (minimizing the piecewise lengths). However, at the key points, the velocity and the acceleration are very costly due to a big change of the geodesic direction and its rate of change (see figure 1, (c) and (d)). Quite the contrary, the two other methods provide smooth paths with smaller accelerations at the key points. More specifically, they lead to roughly the same velocities but the acceleration cost is slightly smaller under the proposed method. The later method leads to better reconstruction results as shown in (figure 1, (e) and (h)) with less sharpness at data points (figure 2, (f) and (g)). In general, the proposed method succeeds to generate smooth fitting paths on Riemannian manifolds for other interesting applications [2].

## 5 Conclusion

We have introduced an efficient method for cylindrical surfaces reconstruction. The input data is obtained as a finite indexed set of level-curves, extracted manually from MRI, in the case of endometriosis. The proposed method reconstructs the surface as a fitting paths on the shape space of planar closed curves by overcoming the main numerical limitations of the standard methods, *i.e.* the regularity and the preservation of the distance function.

## References

[1] P.-A. Absil, R. Mahony, and R. Sepulchre. *Optimization Algorithms on Matrix Manifolds*. Princeton University Press, Princeton, NJ, 2008.

[2] A. Arnould, P.-Y. Gousenbourger, C. Samir, P.-A. Absil, and M. Canis. Fitting Smooth Paths on Riemannian Manifolds : Endometrial Surface Reconstruction and Preoperative MRI-Based Navigation. Preprint, 2015.

[3] C.L. Bajaj, G.-L. Xu, and Q. Zhang. Bio-molecule surfaces construction via a higher-order level-set method. *Journal of Approximation Theory*, 23(6):1026–1036, 2008.

[4] N. Dyn. Linear and nonlinear subdivision schemes in geometric modeling. In Felipe Cucker, Allan Pinkus, and Michael J. Todd, editors, *Foundations of Computational Mathematics*, volume 363, pages 68–92. Cambridge University Press, 2009.

[5] G.E. Farin. *Curves and Surfaces for CAGD*. Academic Press, fifth edition, 2002.

[6] P.-Y. Gousenbourger, C. Samir, and P.-A. Absil. Piecewise-Bézier C1 interpolation on Riemannian manifolds with application to 2D shape morphing. In *IEEE International Conference on Pattern Recognition (ICPR)*, 2014.

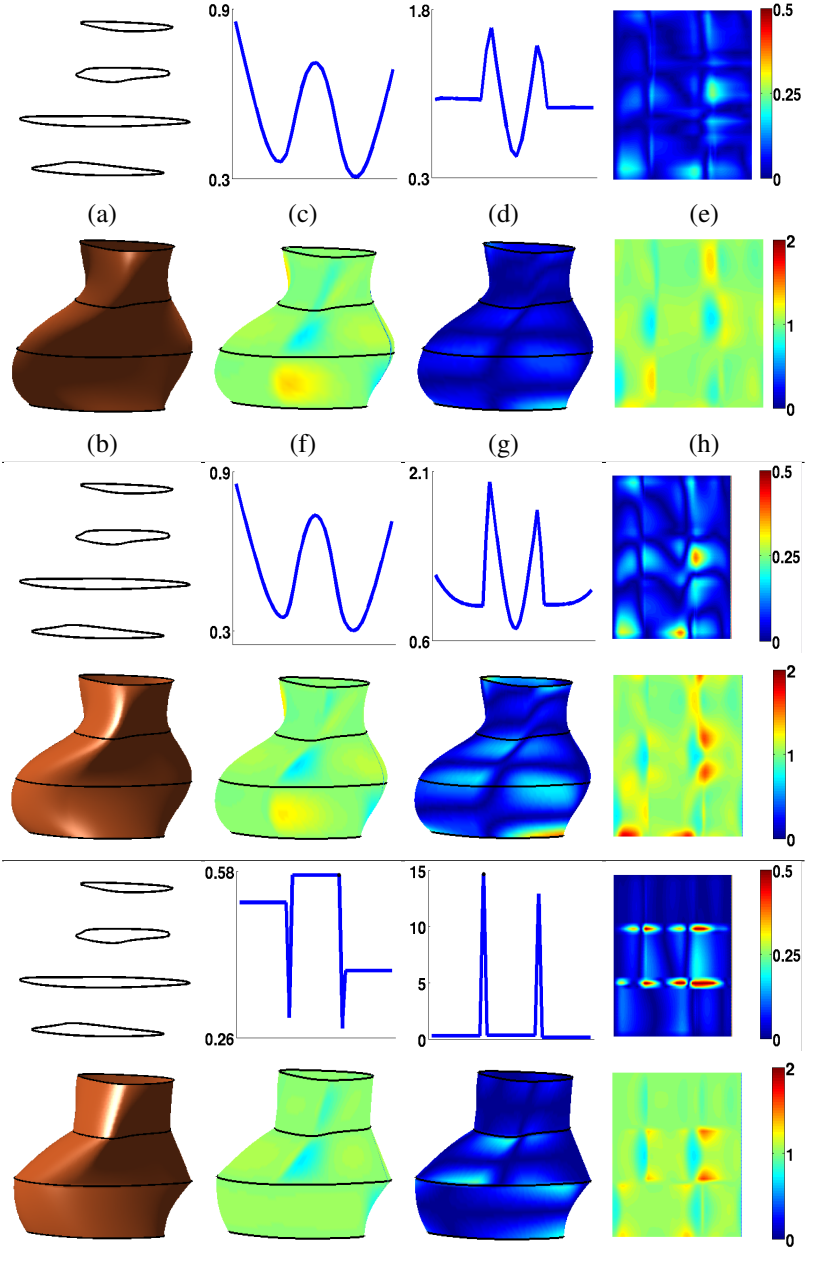


**Figure 1:** a: original curves, b: reconstructed surface $S_{MRI}$, c: $\|\dot{\eta}\|$, d: $\|\ddot{\eta}\|$, e: $\|\nabla^2 S_{MRI}(r,\theta)\|$, f: $\|\nabla_r S_{MRI}(r,\theta)\|$, g: $\|\nabla_\theta S_{MRI}(r,\theta)\|$, and h: $\|\nabla S_{MRI}(r,\theta)\|$. The two first rows correspond to the solution from [2], the two next to the solution from [6] and the last two to piecewise-geodesics.

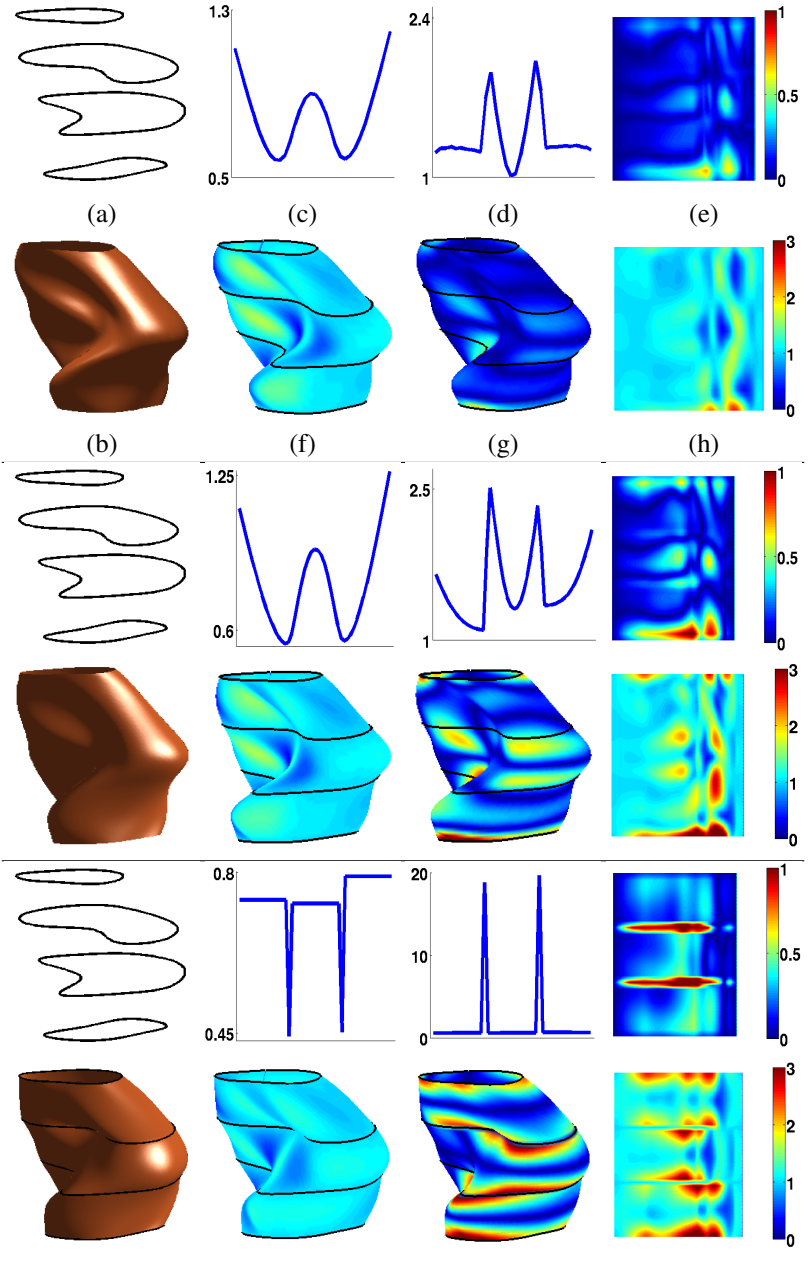


**Figure 2:** a: original curves, b: reconstructed surface $S_{MRI}$, c: $\|\dot{\eta}\|$, d: $\|\ddot{\eta}\|$, e: $\|\nabla^2 S_{MRI}(r,\theta)\|$, f: $\|\nabla_r S_{MRI}(r,\theta)\|$, g: $\|\nabla_\theta S_{MRI}(r,\theta)\|$, and h: $\|\nabla S_{MRI}(r,\theta)\|$. The two first rows correspond to the solution from [2], the two next to the solution from [6] and the last two to piecewise-geodesics.

[7] K. Hüper and F. Silva Leite. On the geometry of rolling and interpolation curves on $S^n$, $SO(n)$, and Grassmann manifolds. *J. Dyn. Control Syst.*, 13:467–502, 2007.

[8] S.H. Joshi, E. Klassen, A. Srivastava, and I. Jermyn. A novel representation for Riemannian analysis of elastic curves in $R^n$. In *IEEE Computer Vision and Pattern Recognition (CVPR), Conference on*, pages 1–7, 2007.

[9] Achan Lin and Marshall Walker. CAGD techniques for differentiable manifolds. *Algorithms for approximation IV. Proceedings of the 2001 International Symposium*, pages 36–43, 2001.

[10] L. Machaldo, F. Silva Leite, and K. Krakowski. Higher-order smoothing splines versus least squares problems on Riemannian manifolds. *Journal of Dynamical and Control Systems*, 16(1):121–148, 2010.

[11] J. Park. Interpolation and tracking of rigid body orientations. In *Control Automation and Systems (ICCAS), International Conference on*, pages 668–673, 2010.

[12] Quentin Rentmeesters. A gradient method for geodesic data fitting on some symmetric Riemannian manifolds. *Proceedings of the IEEE Conference on Decision and Control*, pages 7141–7146, 2011.

[13] C. Samir, P.-A. Absil, A. Srivastava, and E. Klassen. A gradient-descent method for curve fitting on Riemannian manifolds. *Foundations of Computational Mathematics*, 12:49–73, 2012.

[14] O. Sander. Geodesic finite elements of higher order. *IMA Journal of Numerical Analysis*, 2015.

[15] A. Srivastava, E. Klassen, S. H. Joshi, and I. H. Jermyn. Shape analysis of elastic curves in Euclidean spaces. *IEEE Transactions on Pattern Analysis and Machine Intelligence (PAMI)*, 33:1415–1428, 2011.

[16] H.K. Zhao, S. Osher, and R. Fedkiw. Fast surface reconstruction using the level set method. In *IEEE Workshop on Variational and Level Set Methods in Computer Vision (VLSMCV)*, pages 194–201, 2001.